sciendo

DOI 10.2478/ama-2023-0037

acta mechanica et automatica, vol.17 no.3 (2023)
Special Issue "Computational Technologies in Engineering TKI2022"

PROPERTIES OF RUBBER-LIKE MATERIALS AND THEIR BLENDS IN WIDE RANGE OF TEMPERATURES – EXPERIMENTAL AND NUMERICAL STUDY

Marcin KONARZEWSKI*, Michał STANKIEWICZ*, Marcin SARZYŃSKI, Marcin WIECZOREK*, Magdalena CZERWIŃSKA***, Piotr PRASUŁA, Robert PANOWICZ***

*Faculty of Mechanical Engineering, Military University of Technology, ul. gen. Sylwestra Kaliskiego 2, 00-908 Warszawa, Poland
**Faculty of Mechatronics and Aeronautics, Military University of Technology, ul. gen. Sylwestra Kaliskiego 2, 00-908 Warszawa, Poland
***Military Institute of Armament Technology, ul. Wyszyńskiego, 05-220 Zielonka, Poland

marcin.konarzewski@wat.edu.pl, michal.stankiewicz@wat.edu.pl, marcin.sarzynski@wat.edu.pl, marcin.wieczorek@wat.edu.pl, czerwinskam@witu.mil.pl, prasulap@witu.mil.pl, robert.panowicz@wat.edu.pl

received 19 January 2023, revised 24 February 2023, accepted 13 March 2023

Abstract: Elastomers are widely used in many industries. Their use requires thorough knowledge of their strength and stiffness parameters over a wide temperature range. However, determination of the parameters of such materials is still a challenge. Therefore, the paper presents research methodology allowing determination of the properties of rubber-like materials in a wide range of stretch and temperatures (from +50°C to −25°C) by using the example of styrene-butadiene rubber (SBR) and natural rubber (NR) elastomers. Additionally, two blends, chloroprene rubber/nitrile-butadiene rubber (CR/NBR) and NR/SBR blends, were also considered. Based on physical premises, a polynomial and Arruda–Boyce hyperelastic constitutive models parameters were determined using two different methods, namely curve-fitting and the successive response surface method.

Key words: polymers, uniaxial tension, temperature effects, optimisation

1. INTRODUCTION

Elastomers are currently one of the most commonly used material groups in modern industry. Their usage extends from the automotive industry, where they are used mostly for car tires and suspension components, up to civil engineering, aviation and biomechanics.

The determination of the mechanical properties of such materials is crucial due to their wide usage in different industries. Especially, it is very important to take into account the influence of the operating temperature on the change of the mechanical properties [1]. The change of such parameters as tensile strength, stress or stiffness with the temperature change results from the internal structure of rubber-like materials in which polymer chains are joined by intermolecular bonds [2, 3]. The study of this influence is all the more important as, during the tensile tests of such materials, we observe an increase in displacement when the temperature is lowered and not when it is increased, contrary to what might intuitively be hypothesised to be the case [4, 5]. In the case of elastomers, we observe a rapid degradation of the polymer chains at elevated temperatures [6].

There is a whole range of elastomers differing significantly in their mechanical properties and, thus, their usage [7]. The presented article focuses on several commonly used materials and blends, namely styrene-butadiene rubber (SBR), natural rubber (NR), and NR/SBR and chloroprene rubber/nitrile-butadiene rubber (CR/NBR) blends.

SBR is a synthetic copolymer consisting of styrene and butadiene [8]. Due to its properties, it is widely used in the automotive tires industry and for various parts of car interiors [9]. Owing to the addition of the styrene, the strength, abrasion resistance and blend properties of butadiene are improved [10]. On the other hand, the SBR is vulnerable to thermal and oxidative degradation due to the presence of double bonds in the polydiene backbone. This process manifests itself by an increase in stiffness of the material due to the cross-linking [11]. The typical operating temperature of SBR is in a range between -50°C and 100°C.

NR is one of the oldest materials known to man, but only the discovery of the vulcanisation process caused the rapid development of the rubber processing industry [12]. The main application of NR is in the truck tire industry, because of its high tear resistance, toughness and high tensile strength [13]. Additionally, NR is chemically stable, except for oils. However NR is also characterised by low thermal resistance and low organic solvent resistance, and thus various chemical modifications are required in some cases of usage [14].

Chloroprene rubber (CR) is a synthetic material created in the process of polymerisation of chloroprene [15]. This material is characterised by high resistance to weather conditions, to ozone and even to weak acids. Due to high chemical stability, it is relatively well resistant to aging [16].

Nitrile-butadiene rubber (NBR), which is a copolymer of acrylonitrile and butadiene, is characterised by an excellent resistance to a wide range of oils of mineral, animal and vegetable origin as well as to fuels and other chemicals [17]. It is an elastic material with a high tensile strength and a low compression deformation [18]. For this reason, it is frequently used in the automotive or aviation industry, to produce seals (for both hydraulic and pneumatic installations), vibration damping elements and self-sealing fuel tanks.

In order to improve the properties of rubber-like materials, the technology of polymer–polymer blends was extensively researched. Development of the multi-component systems allowed for enhancing the properties, especially mechanical, of polymeric materials [19]. One of the most commonly used materials is the above-mentioned rubber, which – due to its properties (especially high tensile strength) – is commonly blended with synthetic rubbers [19, 20]. In the case of the NR/SBR blends, the main advantage is improved oxidative stability [21], whereas in case of the CR/NBR blend, an increase in the mechanical properties is observed [22].

In the literature, a description of a series of constitutive material models that can be used to describe the behaviour of elastomers can be found. They include, among others, the Mooney–Rivlin model, neo-Hookean, Gent–Thomas, Yeoh, polynomial and Arruda–Boyce [23]. The greatest difficulty in their use is the need to have a set of appropriate material parameters. Since the mechanical properties of this type of materials are strongly influenced by e.g. the ambient temperature, one universal data set covering the entire temperature range is insufficient to correctly describe the material's behaviour under operating conditions. It is necessary to conduct experimental tests in the required temperature range, and then use the obtained data to determine the required parameters of the constitutive model. In order to determine the aforementioned parameters, usually a tensile or compression test is carried out. The stress–strain curve obtained as a result of the tests then forms the basis for determining the parameters using the curve-fitting technique. In this method, in subsequent iterations, the values of the parameters are being substituted, and then the resulting output curve is compared with the input curve. The iterations are repeated until the desired convergence is obtained, usually determined by the value of R-squared, which is a statistical metric used to evaluate the degree to which variations in the dependent variable, which is the target of the analysis, are accounted for by variations in the independent variables, which are the predictors. It is a ratio expressed as a value between 0 and 1, where a higher value indicates that the model explains a larger proportion of the variance in the dependent variable, and a value of 0 indicates that the model does not explain any of the variance.

The article aimed mainly to show the change in properties and to determine the constitutive models' parameters of various elastomers such as SBR and NR rubbers and their blends, NR/SBR and CR/NBR, in a wide range of temperatures. Both the experimental and numerical approach were utilised during the research. The experimental research allowed for determining the glass transition temperatures with use of the both dynamic mechanical analysis (DMA) and differential scanning calorimetry (DSC) methods. The tensile tests allowed for determination of the change in the stiffness and the fracture energy of the tested materials in conditions of both lowered and increased ambient temperatures (ranging from -25°C up to 50°C). The selected temperature range corresponds to the typical operating conditions of such materials. During the tests in the negative temperature, the crystallisation process was observed for NR material. Additionally, in the case of the NR/SBR blend, a crystallisation of the NR component can be witnessed at low temperatures, which indicates that this blend is characterised by a low miscibility.

The results of the experimental tests served as the basis on which, using the curve-fitting method, the material constants of two commonly used hyperelastic constitutive models – polynomial and Arruda–Boyce – were determined for the presented temperature range. The obtained values were also verified numerically using the finite element method and the results were compared with the experimental tests. By means of application of the successive response surface method (SRSM), the optimisation process of the previously obtained values was carried out. It was found that in most cases the true-strain vs. true-stress curve representing the polynomial model coincides with the average curve obtained from experimental tests, whereas for the Arruda–Boyce material model the discrepancies are greater. The average difference between the values obtained from the Arruda–Boyce model and experimental tests is about 16%, whereas for the polynomial model the difference is about 4%.

In practice, especially in numerical analysis, rubber materials are assumed to be practically incompressible. For this reason, a significant proportion of hyperelastic models are able to correctly predict the behaviour of the material in different deformation states (e.g. tensile, biaxial tension or compression). Therefore, only the tensile test curves were used for curve-fitting and parameter determination. It should be noted, however, that the use of the presented parameters in deformation states other than uniaxial stress may lead to slight inaccuracies.

Such a large database of parameters – covering both a wide range of different materials and taking into account the high variability of thermal conditions – gathered in one place is an extremely large help for all those interested in the most accurate numerical modelling of construction elements made of elastomers.

2. MATERIALS AND METHODS

2.1. Specimen preparation

In order to conduct the research, commercially available materials were selected, namely SBR and NR, and two additional blends, NR/SBR and CR/NBR. Materials were obtained from the manufacturer in the form of 300 mm × 300 mm and 2 mm thick sheets. Prior to preparing specimens, the hardness of the materials was measured using the Shore A scale at a temperature of 21°C. The values of the hardness are in the range from 61 to 64. Accordingly, all tested materials have a comparable hardness at ambient temperature and can be classified as rather hard rubbers. The exact composition of the tested materials and results of the hardness measurements are presented in Tab. 1.

The dimensions of the samples were determined based on the PN-ISO 37:2007 standard concerning the determination of the tensile properties of rubber (Fig. 1). The water jet cutting technique was used to prepare the test samples. In order to minimise deformation caused by the water jet cutting process, the material sheets were clamped between two steel plates during the cutting operation. Due to the low stiffness exhibited by all the tested materials, it was not feasible to perform machining on their surfaces to enhance their parallelism accuracy. An example of the prepared samples is presented in Fig. 2.

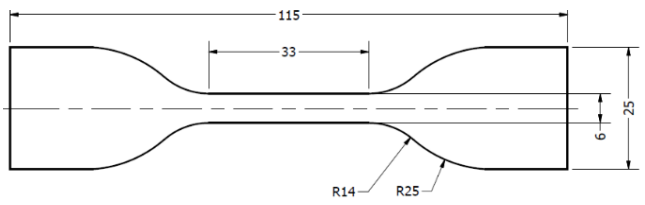

Fig. 1. Dimensions of the test samples according to the PN-ISO 37:2007 standard

Tab. 1. Composition of tested materials

Component (phr)	CR/NBR	NR	SBR	NR/SBR
NR (RSS I)	-	100	-	50
CR (Denka S-40)	50	-	-	-
Acrylonitrile-butadiene rubber (Perbunan 1847)	50	-	-	-
SBR (Ker 1500)	-	-	100	50
Carbon black (N-550)	83.3	40	50	45
Cross-linking complex (sulphur, ZnO and others)	-	20	13.8	19
Cross-linking complex (MgO, ZnO and others)	13.8	-	-	-
Softener (ADO or AN-68*)	27	7*	10*	12
Hardness Shore A (at 21°C)	64	62	61	64

* AN-68 softener
phr, weight parts per 100 parts of rubber.
CR, chloroprene rubber; NBR, nitrile-butadiene rubber; NR, natural rubber; SBR, styrene-butadiene rubber.

White paint markers were applied on every sample in the measuring part. They were necessary to determine the deformations of the samples during the tensile test using a motion tracking method.

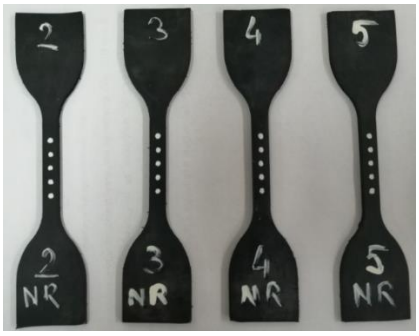

Fig. 2. Example of the test samples. NR, natural rubber

2.2. DMA

DMA is one of the most frequently used methods for determining the viscoelastic properties of materials. Generally, in this method, a sinusoidal force (stress) is applied to the sample, which results in a sinusoidal deformation (strain). In case of the viscoelastic materials, the shift in the corresponding stress and strain curves is observed. The phase difference between those curves is called phase angle or phase lag δ [24].

From the DMA tests, several viscoelastic terms can be calculated [25]:

$$E' = (\sigma_0/\varepsilon_0) * \cos\delta \quad (1)$$

$$E'' = (\sigma_0/\varepsilon_0) * \sin\delta \quad (2)$$

$$\mathrm{Tan}\,\delta = E''/E' \quad (3)$$

where E' is the storage (elastic) modulus, E'' is the loss (viscous) modulus, tan δ is an index of viscoelasticity (loss factor), σ_0 is the maximum applied stress, ε_0 is the maximum strain amplitude and δ is the phase angle. The storage modulus is a measure of elastic energy stored in the material, the loss modulus measures the energy dissipation during each cycle of the loading and tan δ is a ratio of the two previously mentioned values.

DMA was performed by using TA Instruments' DMA Q800 analyser. Strips in dimensions of 55 mm × 10 mm × 3 mm (length × width × thickness) were used as samples. They were made in the same way as the tensile test specimens, using a water jet cutter. A dual cantilever clamp was used to examine the thermo-mechanical properties. The storage and loss modulus and tan δ were measured at a frequency of 1 Hz over a temperature range of –90°C to 50°C at a heating rate of 5°C/min. The amplitude of test sample deformation was established at 20 μm.

2.3. DSC

Another commonly used thermal test method is DSC [26]. The main principle of the method is to heat a sample of a known mass and track changes in its heat capacity as changes in the heat flow [27]. Typically, the test sample is enclosed in the pan and mounted inside the furnace on the thermoelectric disk. The empty reference pan is also present [24]. Throughout the test procedure, the temperature inside the furnace is changed at a constant rate, the temperature difference ΔT between the samples is measured and recorded, and then the heat flow is determined based on the following expressions [28]:

$$\mathrm{q} = \Delta\mathrm{T}/R \quad (4)$$

$$\mathrm{q} = c_p(dT/dt) + f(T,t) \quad (5)$$

where q is sample heat flow, ΔT is the temperature difference between the samples, *R* is the resistance of the thermoelectric disk, c_p is sample-specific heat capacity, *dT/dt* is a heating rate and *f(T, t)* is kinetic response at a specific temperature and time.

A DSC Q250 calorimeter from TA Instruments with Refrigerated Cooling System RCS90 was used to perform the DSC analysis. Measurements were carried out in an inert gas atmosphere (nitrogen) at a heating rate of 10°C/min, in the range from –80°C to 70°C, using non-hermetic aluminium pans. During the tests, the glass transition temperature was obtained.

2.4. Tensile test

In order to perform the tensile tests, an MTS Criterion Model 45 electromechanical universal test system was used. The system is characterised by a maximum displacement range of ±500 mm and the maximum piston speed is 750 mm/min. Additionally, the ThermCraft temperature chamber was utilised to perform tests in both negative and positive temperatures.

The tensile test was carried out based on the PN-ISO 37:2007 standard with the speed of the traverse of 50 mm/min. The strain rate during the tests was constant and equal to $3.3 \cdot 10^{-2} \cdot s^{-1}$. The force and the position of the transverse were recorded with 50 Hz frequency. Additionally, the motion tracking method was used in order to determine the strain of the test samples. For this purpose, every test was recorded using a high-resolution camera (1,920 × 1,080 pixels). In the next step, recordings were imported into TEMA software, which allowed for tracking the points painted on the samples and recording their position-change over time.

Recorded coordinates were the basis for calculation of the strain. The stress was calculated as the loading force related to the initial cross-section area of the tested sample. The effect of transverse deformations of the sample during the test was not taken into account.

The samples were tested in the following temperatures: –25°C, 0°C, 25°C and 50°C. Prior to the tests, the samples were placed in the chamber for 1 h in the test temperature. After that, the samples were sequentially mounted in the clamps of the testing system and an additional 15 min was allowed to pass for the samples' settling and temperature-normalisation. The tests were performed when the control system was showing constant, set temperature. Temperature measurements were obtained using two K type thermocouples – one located within the working field of the chamber, and another inserted between two layers of the test material. To obtain the latter, two pieces of the test material were placed in contact, with the thermocouple inserted between them. The tests were carried out once the control system indicated a constant, predetermined temperature. The chamber specifications indicated that the temperature stabilisation accuracy was within ±1°C, whereas the acceptable error range for the K type thermocouples was ±1.5°C.

3. RESULTS AND DISCUSSION

3.1. DMA

The DMA allowed us to investigate two-component rubber compounds and their interactions. The storage modulus value of the NR in the below-Tg plateau region is considerably higher than for any other considered elastomer and equal to 21,310 MPa, whereas for SBR it is only 8,640 MPa (the lowest value of all considered samples) (Fig. 3a). The addition of the NR to SBR causes a slight increase in its value to 9,215 MPa and considerable widening of the glass transition by approximately 57% (onset at –56°C, termination at –27°C). Additionally, the course of the storage modulus curve in the glass transition temperature is not linear, and a slight change in the slope can be observed at approximately –44°C. It indicates the two-phase structure of the NR/SBR blend, and thus a low miscibility of the individual components. The glass transition temperature of the NR is equal to –51.7°C, which is a similar value to that obtained for the CR/NBR blend, whereas in the case of the SBR it is –40.7°C. The blend of those two components shows a slightly lower Tg of about –56.2°C.

Analysing the storage modulus of the CR/NBR blend, we can observe that at –90°C, its value attains 15,830 MPa and is 71% higher than that corresponding to the NR/SBR blend. The change in stiffness is more pronounced than in the NR/SBR blend. The onset of the glass transition is observed at a relatively low temperature of –80°C, whereas termination at –30°C. The glass transition temperature is –55.8°C.

Concerning the cases of the NR, SBR and their blend, we can make the common observation that the peak value of the loss modulus of the NR (4,340 MPa at –45.5°C) is considerably higher compared with the corresponding values for other materials, due to its storage modulus having a high value (Fig. 3b). The SBR peak value is equal to 1,420 MPa at –32.3°C. The NR/SBR blend is characterised by two clearly visible peak values in both loss modulus and tan δ curves, corresponding to the values of the glass transition temperature of individual NR and SBR rubber. Such behaviour proves that individual components of the blend are rather immiscible.

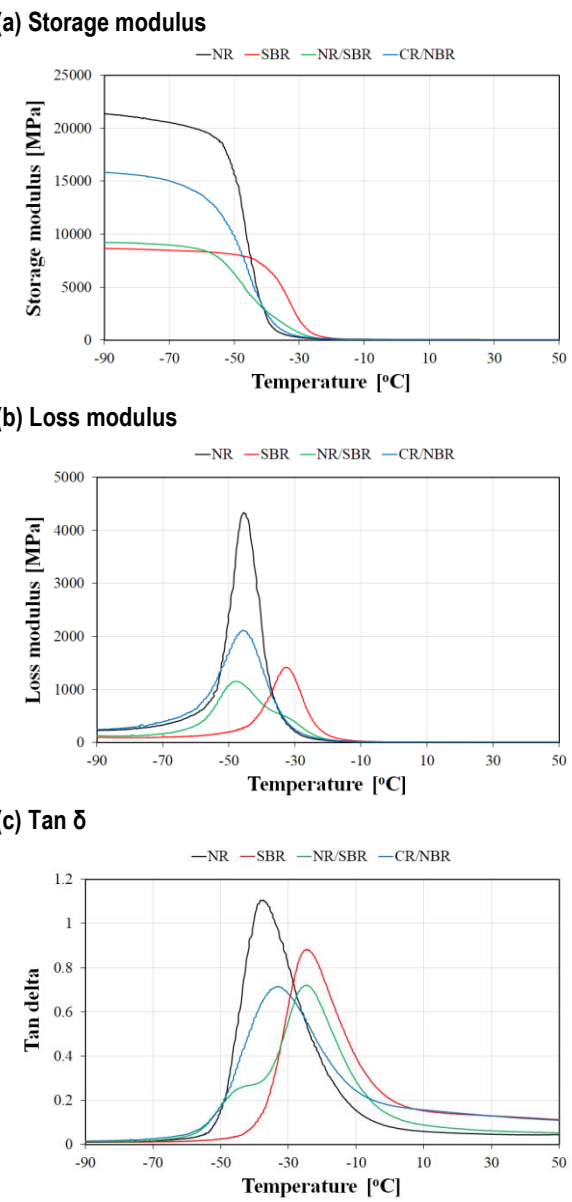

Fig. 3. Values of: a) storage modulus, b) loss modulus and c) tan δ modulus received by DMA. CR, chloroprene rubber; DMA, dynamic mechanical analysis; NBR, nitrile-butadiene rubber; NR, natural rubber; SBR, styrene-butadiene rubber.

In the case of the CR/NBR blend, the lost modulus peak value is equal to 2,115 MPa at a temperature of –45.7°C (Fig. 3b). Additionally, only one peak is observed, which proves the good miscibility of the blend components. In the case of the tan δ, for the CR/NBR, the maximum value is equal to 0.71 at –33.1°C (Fig. 3c). Analogically as in the loss modulus curve, only one peak is visible.

The values of the glass transition temperature (Tg) of rubber were estimated based on the temperature DMA curves and are presented in Tab. 2.

Tab. 2. The glass transition temperatures of rubbers received by DMA

Glass transition temperature Tg (°C)			
	E′	E″	Tan δ
NR	–51.7	–45.5	–37.4
CR/NBR	–55.8	–45.7	–33.1
SBR	–40.7	–32.3	–24.7
NR/SBR	–56.2	–48.4 –32.7	–32.7 –24.5

CR, chloroprene rubber; DMA, dynamic mechanical analysis; NBR, nitrile-butadiene rubber; NR, natural rubber; SBR, styrene-butadiene rubber.

3.2. DSC

The thermograms for all considered materials are presented in Fig. 4. The obtained results allow the conclusion that for all samples except NR/SBR, the glass transition process was one-stage. In the case of sample NR/SBR, a two-stage incidence of the glass transition process was observed, due to the presence of two immiscible components with different glass transition temperatures. In the case of the CR/NBR blend, we can observe a single-stage thermal conversion, which can be an indication of the good miscibility of the blend components. The glass transition temperatures obtained by DSC are presented in Tab. 3.

The test results obtained by DSC confirm the results gained based on analysis performed by DMA, and thus the behaviour of CR/NBR and NR/SBR blends.

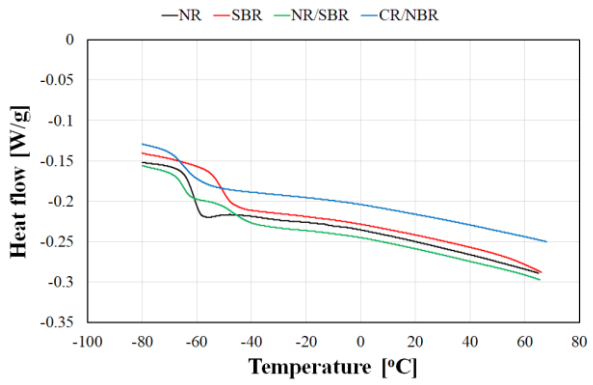

Fig. 4. DSC thermograms for considered rubbers. CR, chloroprene rubber; DSC, differential scanning calorimetry; NBR, nitrile-butadiene rubber; NR, natural rubber; SBR, styrene-butadiene rubber.

Tab. 3. The glass transition temperatures of rubbers received by DSC

Glass transition temperature Tg (°C)			
	T_{onset} (°C)	$T_{midpoint}$ (°C)	T_{end} (°C)
NR	–64.6	–61.4	–58.7
CR/NBR	–69.0	–64.2	–59.3
SBR	–54.5	–50.4	–46.1
NR/SBR	–67.9 –51.3	–65.2 –46.3	–62.4 –41.4

CR, chloroprene rubber; DSC, differential scanning calorimetry; NBR, nitrile-butadiene rubber; NR, natural rubber, SBR, styrene-butadiene rubber.

3.3. Tensile tests

In Fig. 5, an example of the test sample during the tensile test in the elevated temperature is presented.

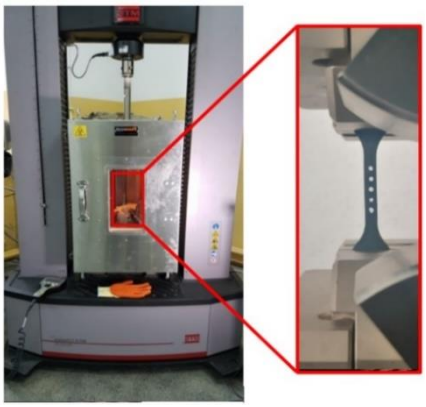

Fig. 5. Example of the specimen during the tensile test at 50°C

The stress (σ)-extension ratio (λ) plots for all tested materials at the ambient temperature are presented in Fig. 6. Extension ratio is defined as:

$$\lambda = \varepsilon + 1 \tag{6}$$

where ε is an engineering strain.

It can be observed that all the curves are located in a relatively narrow range in all considered cases. The standard deviation of maximum extension ratio at ambient temperature is 0.16 for CR/NBR, 0.23 for SBR, 0.41 for NR and 0.42 for NR/SBR.

(a) CR/NBR

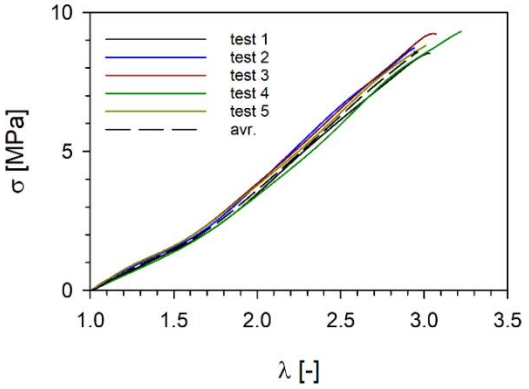

(b) NR

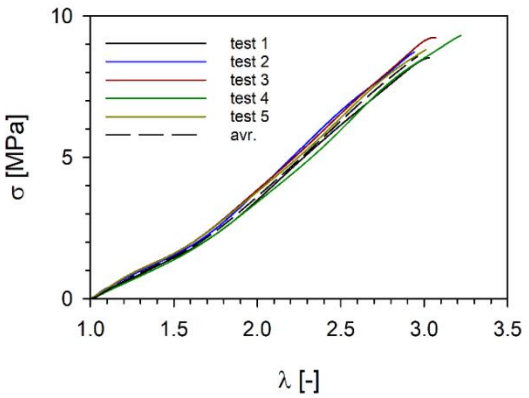

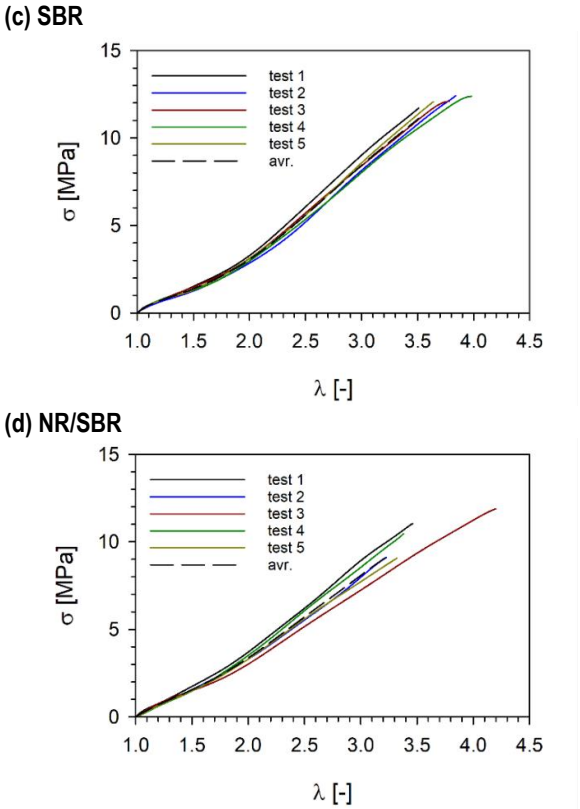

Fig. 6. Stress-extension ratio curves for tests at the ambient temperature: (a) CR/NBR, (b) NR, (c) SBR, (d) NR/SBR. CR, chloroprene rubber; NBR, nitrile-butadiene rubber; NR, natural rubber; SBR, styrene-butadiene rubber.

The averaged curves of stress-extension ratio for tests performed in the considered range of temperatures are presented in Fig. 7.

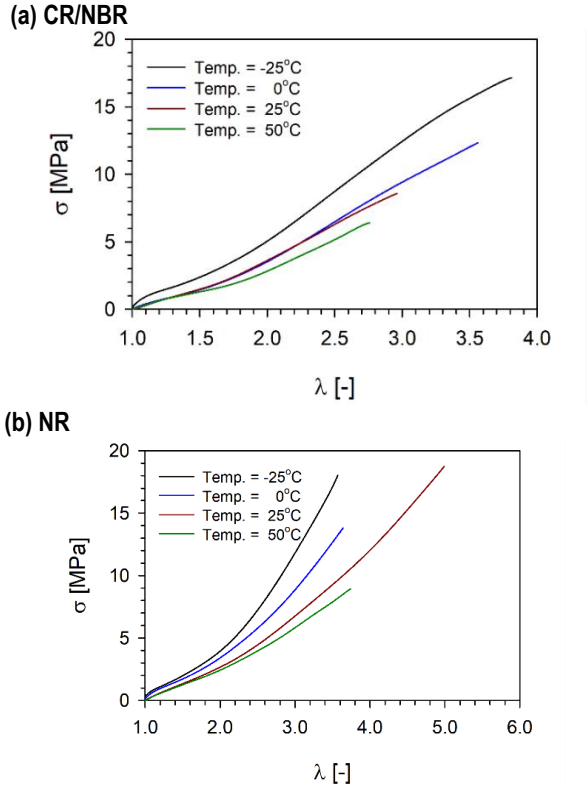

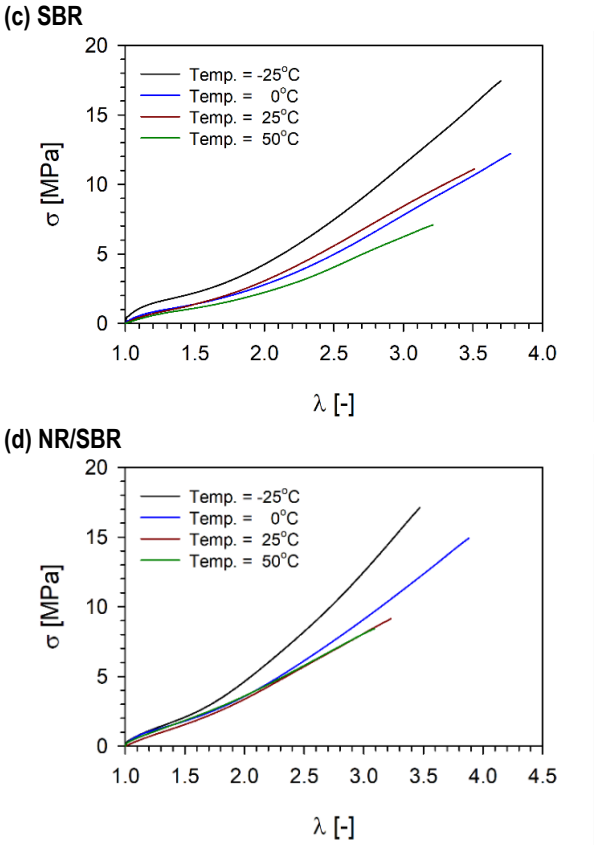

Fig. 7. Stress-extension ratio curves for for a wide range of temperatures: (a) CR/NBR, (b) NR, (c) SBR, (d) NR/SBR. CR, chloroprene rubber; NBR, nitrile-butadiene rubber; NR, natural rubber; SBR, styrene-butadiene rubber.

In the case of the CR/NBR blend, the stiffness values at 0°C and 25°C are almost identical up to an extension ratio of 2.5 (Fig. 7a). Although both of the blend components are characterised by the upturn in the stress, no such behaviour is observed for the CR/NBR. The mechanical behaviour of the blend can somewhat be visualised as a mixture of the properties of its components, i.e. unlike in the NBR, there is no rapid change in the material stiffness at –25°C, whereas the maximum stress values are lower than those obtained for the CR. For the temperature of 50°C, the maximum stress value was equal to 6.5 MPa, whereas for –25°C it was higher and equal to 17 MPa.

In the case of NR, we can observe that curves for ambient temperature and 50°C coincide to the value of the extension ratio of 1.6, whereas other curves have different slopes (Fig. 7b). Two phenomena related to crystallisation can be observed. The first one is strain-induced crystallisation. High deformations result in a change of molecular orientation of its network, whereas the induced crystallites slow down the crack growth [29]. The second phenomenon is the ability to crystallise in the un-stretched state in the lowered temperatures, the so-called thermally induced crystallisation (TIC). As a previous research showed, the maximal crystallisation rate takes place at approximately –25°C [30]. These two behaviours are especially visible in the stress-extension ratio for –25°C when a rapid change in the slope is observed at $\lambda = 2.2$. Analogically as in other considered cases, the lowest value of stress (9 MPa) was obtained at 50°C.

For the SBR material, we can observe that initially the curves in the temperature-range from 0°C to 50°C coincide, but com-

mencing from the extension ratio λ = 1.5, the slope of the 50°C curve changes (Fig. 7c). The curves for 0°C and 25°C continue to coincide until the extension ratio reaches the value of 1.75, but even after that, the value of stress in both cases remains at a very similar level. Analogically as in the case of the NBR, we can observe a change in the stiffness and strength of the SBR at –25°C; however, the maximum stress value is lower and equal to 17.5 MPa. The lowest value of 7 MPa was obtained at 50°C. A slight upturn in the stress is visible in the range from 50°C to 0°C, whereas for –25°C it is significantly more pronounced. As indicated in a previous research, when there is an absence of the crystallisation effect in the SBR rubbers, such behaviour can be explained by the limited extensibility of the network [31].

The NR/SBR blend is characterised by a stiffness that is almost identical at both 25°C and 50°C (Fig. 7d). Additionally, the curve for 0°C coincides with the curves for 25°C and 50°C up to an extension ratio of 2.3. The lowest value of the stress was obtained for 50°C (8.5 MPa), but it was only slightly lower than the stress for 25°C (9.2 MPa). The highest value of 17 MPa was obtained for 50°C. Particularly worth noting is the fact that for the temperature range from 0°C to 50°C, the curves have a single-phase nature, without the visible onset of the stress value. For –25°C, the two-stage characteristic is clearly visible. It is caused by the crystallisation process in the NR component of this low-miscible blend, due to the strain and low temperature.

The influence of the temperature on the material samples' stretching process is also presented in Fig. 8. It shows a relationship between the stress and the temperature for selected extension ratio values. The observed variation exhibits almost monotonic behaviour. In the case of CR/NBR and SBR, a deviation from this trend is evident at 25°C, resulting in an increase in stress values. Conversely, the NR/SBR blend demonstrates a slight increment in stress at 50°C.

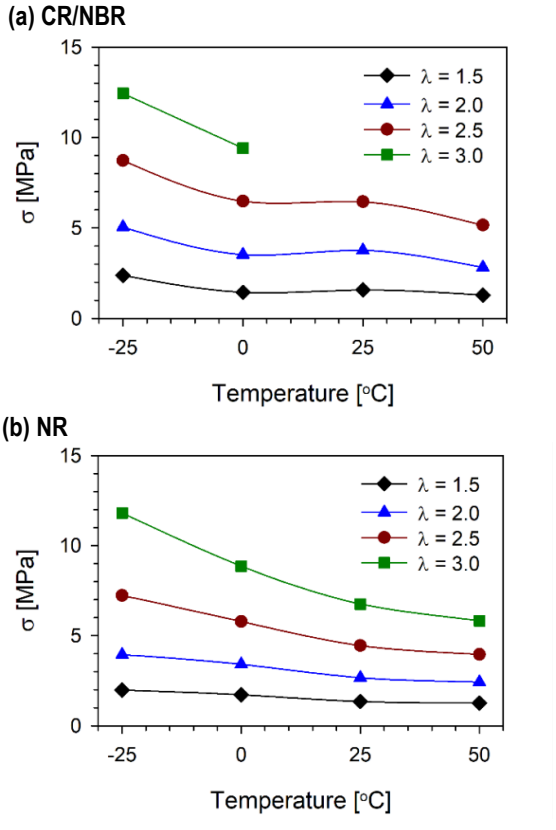

Fig. 8. The stress-temperature curve for different values of extension ratio: (a) CR/NBR, (b) NR, (c) SBR, (d) NR/SBR. CR, chloroprene rubber; NBR, nitrile-butadiene rubber; NR, natural rubber; SBR, styrene-butadiene rubber.

The change in fracture energy Wf is presented in Fig. 9. The fracture energy is calculated as the area below the stress–strain curve. For a given temperature and for a particular material, stress–strain curves obtained from the tensile test of multiple samples were consolidated into a single curve. Subsequently, the area beneath the consolidated curve was determined via a numerical integral algorithm and Excel. It can be observed that the decrease in its value is steady in the whole temperature range. Only in the case of the NR/SBR blend is a rapid decrease observed in the 0–25°C area.

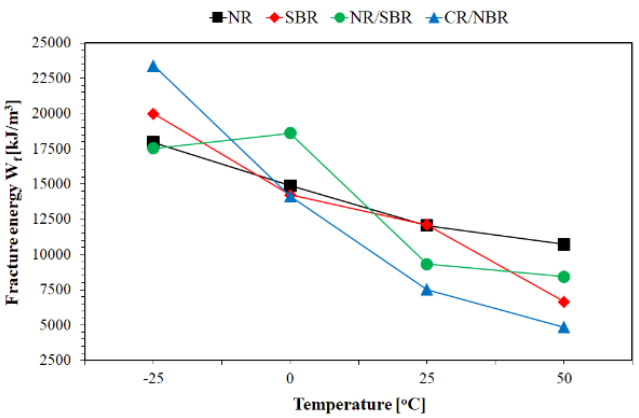

Fig. 9. Fracture energy at various temperatures. CR, chloroprene rubber; NR, natural rubber; NBR, nitrile-butadiene rubber; SBR, styrene-butadiene rubber

In order to better understand the tensile test method results, a so-called Mooney–Rivlin plot can be used [32]. The basis of this plot is the Mooney–Rivlin equation [33,34]:

$$\sigma = 2\left(C_1 + \frac{C_2}{\lambda}\right)\left(\lambda - \frac{1}{\lambda^2}\right) \tag{7}$$

where C_1 and C_2 are material constants and λ is the extension ratio. These constants are associated with the intermolecular forces between the polymer chains and C_1 is related to the crosslink density for elastomers without fillers [35]. Eq. (6) can be rewritten using the term of reduced stress σ^* [32]:

$$\sigma^* = \frac{\sigma}{\lambda - \frac{1}{\lambda^2}} \tag{8}$$

The Mooney–Rivlin plots were constructed by plotting the reduced stress σ^* against the inverse extension ratio $1/\lambda$ and are presented in Fig. 10. Three regions of strain can be distinguished on the plots: low strain ($1/\lambda$ >0.8), intermediate strain and high strain (generally $1/\lambda$ <0.4, but the border value may vary from material to material). Generally, at low strain, the reduced stress decreases up to a certain value, after which it starts to grow, which is associated with the limited chain extensibility between crosslinks (in the non-crystallisable rubbers) and strain-induced crystallisation [36]. Analysing those plots, we can clearly observe that practically in every considered case, the material is characterised by a linear curve in the intermediate strain range at 25°C and above. The only exception is CR/NBR blend, where such behaviour is observed only at 50°C. In the high strain, an upturn is visible in every material at every considered temperature. In the case of NR, the upturn is caused mainly by strain crystallisation. In the case of the non-crystallisable rubbers, the extensibility is reduced due to the presence of the filler (i.e. carbon black). As a result of the interactions between the rubber chains and the filler particles, a bound rubber is formed. The 'tightly bounded rubber' and 'loosely bounded rubber' can be distinguished. The tightly bounded rubber is characterised by low elasticity and high strength [37]. Additionally, some rubber chains are trapped in the filler aggregates and act as part of the filler, thus effectively increasing the volume of the filler and the high strain modulus [38]. In all cases, the reduced stress value increases with the temperature decrease.

In Fig. 11, the upturn strain values are presented. The upturn strain was defined as the strain corresponding to the minimum reduced stress. It is worth noting that in all considered materials, a rapid decrease in the upturn strain at 25°C is observed. At 50°C the value increases again.

(a) CR/NBR

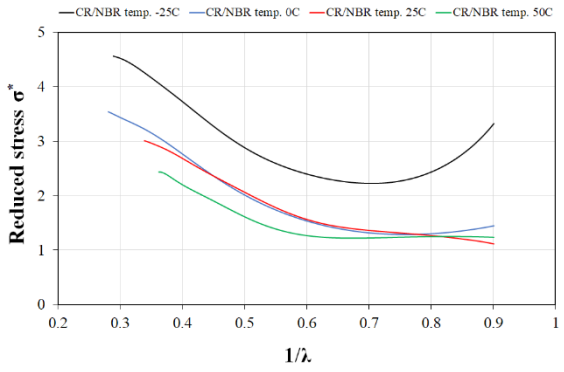

(b) NR

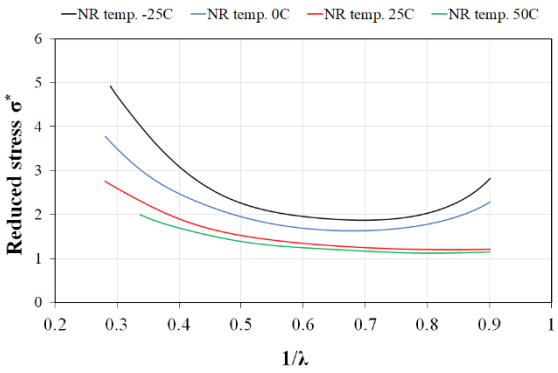

(c) SBR

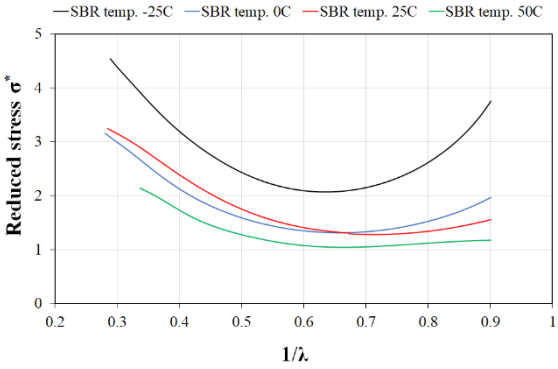

(d) NR/SBR

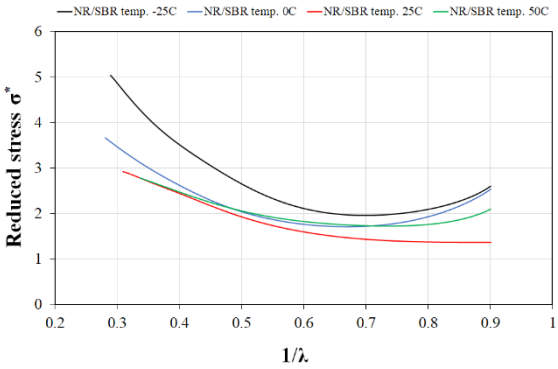

Fig. 10. Mooney–Rivlin plots for the considered materials: (a) CR/NBR, (b) NR, (c) SBR, (d) NR/SBR. CR, chloroprene rubber; NBR, nitrile-butadiene rubber; NR, natural rubber; SBR, styrene-butadiene rubber.

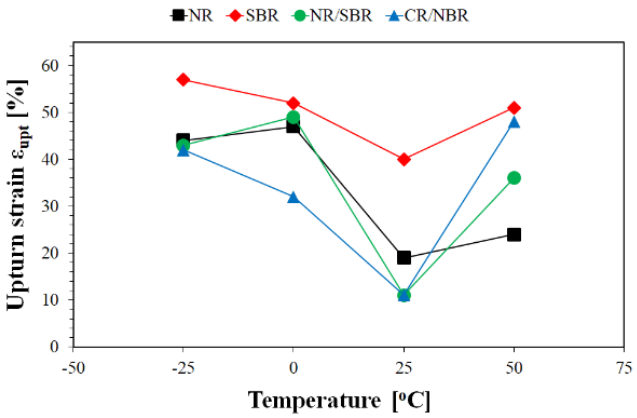

Fig. 11. Values of upturn strain at various temperatures. CR, chloroprene rubber; NBR, nitrile-butadiene rubber; NR, natural rubber; SBR, styrene-butadiene rubber

DOI 10.2478/ama-2023-0037

Similar effects are also seen in Fig. 12. Stress-extension ratio curves for 0°C and 25°C temperatures are presented for all tested materials. It can be observed that in the case of 25°C, all curves are located in a relatively narrow range. Additionally, the extension ratios of all materials in the ambient temperature are practically equal (λ = 3), except the NR material, which is characterised by the highest extension ratio (λ = 5).

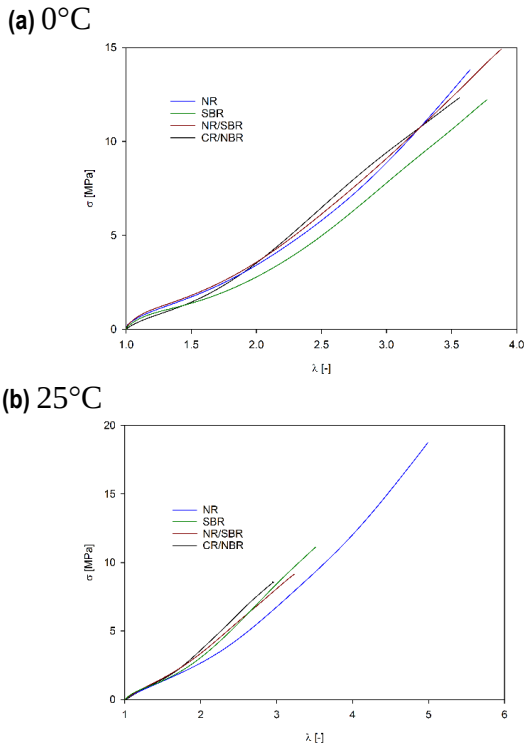

Fig. 12. Stress-extension ratio curves for (a) 0°C and (b) 25°C temperatures. CR, chloroprene rubber; NBR, nitrile-butadiene rubber; NR, natural rubber; SBR, natural rubber.

4. NUMERICAL MODELLING

4.1. Hyperelastic constitutive models

The behaviour of hyperelastic material, which is frequently assumed to be incompressible, is usually described trough of the Cauchy stress tensor [39]:

$$\tilde{\sigma} = -p\tilde{I} + 2\left(\frac{\partial W}{\partial I_1} + I_1\frac{\partial W}{\partial I_2}\right)\tilde{B} - 2\frac{\partial W}{\partial I_2}\tilde{B}^2 \tag{9}$$

where p is pressure, $\tilde{B} = FF^T$ is the left Cauchy–Green tensor, F is a deformation gradient tensor, I_i (i = 1, 2, 3) are strain invariants, W is a strain-energy function dependent on strain invariants $W(I_1, I_2, I_3)$ and $\tilde{I}$ is an identity tensor.

The left Cauchy–Green tensor is defined as:

$$\tilde{B} = FF^T \tag{10}$$

where F is the deformation gradient tensor.

The assumption of rubber incompressibility also limits the number of variables on which strain-energy functions depend (I_3 = 1, to $W(I_1, I_2)$).

Strain-energy functions should allow reflecting the behaviour of hyperelastic material, including dependence on symmetry, thermodynamic, energetic and entropic considerations in the whole range of extension ratio variability. Functions should also meet certain conditions [40]:

– energy vanishes in the undeformed configuration:

$$W|_{I_1=3} = 0 \tag{11}$$

– strain-energy functions and stress tend to infinity at very large deformation:

$$\lim_{\lambda_i\to 0} W = +\infty, \lim_{\lambda_i\to 0}\frac{\partial W}{\partial \lambda_i} = -\infty, \tag{12}$$

$$\lim_{\lambda_i\to +\infty} W = +\infty, \lim_{\lambda_i\to +\infty}\frac{\partial W}{\partial \lambda_i} = +\infty, \tag{13}$$

– stress is equal to 0 in the undeformed configuration and strain-energy functions achieve a minimum:

$$\left.\frac{\partial W}{\partial \lambda_i}\right|_{\lambda_1=\lambda_2=\lambda_3=1} = 0,$$

$$\left.\frac{\partial^2 W}{\partial \lambda_i^2}\right|_{\lambda_1=\lambda_2=\lambda_3=1} > 0, \tag{14}$$

$$det\left[H_{ij}\right] > 0,$$

where H_{ij} is a Hessian matrix and i, j = 1, 2, 3 and λ_i is the principal stretch ratio.

Numerous articles are devoted to the problems associated with the definition of strain-energy functions. These articles present a phenomenological approach [39, 40], a theoretical approach using statistical mechanics of molecular chains network [41, 42] or a mixed approach.

Based on the kinetic theory of elasticity developed by Wall, Treloar defined the simplest form of strain-energy functions, commonly known as the neo-Hookean model [43]:

$$W = \frac{\mu}{2}(I_1 - 3) \tag{15}$$

where μ is the shear modulus.

The value of the shear modulus is related to the temperature and chain density dependence [43]:

$$\mu = nkT \tag{16}$$

where k is the Boltzmann constant, T is temperature and n is chain density.

Arruda and Boyce [42], using a phenomenological approach, developed a model with other material constants dependent on temperature assuming their linear temperature dependence:

$$\lambda_{chain} = \sqrt{\frac{I_1}{3}} \tag{17}$$

$$\beta = L^{-1}\left(\frac{\lambda_{chain}}{\sqrt{n}}\right) \tag{18}$$

$$W = NkT\sqrt{n}\left[\beta\lambda_{chain} - \sqrt{n}\ln\left(\frac{sinh\beta}{\beta}\right)\right] \tag{19}$$

where n is the number of chain segments, T is temperature, k is the Boltzmann constant, N is the number of chains in the network

of a cross-linked polymer, I_1 is the first invariant of the left Cauchy–Green strain tensor and L^{-1} is the inverse Langevin function.

The Arruda–Boyce model can be expressed also in the following form, which is often implemented in the finite element method software [40]:

$$W = G\left[\frac{1}{2}(\bar{I}_1 - 3) + \frac{1}{20N}\left(\bar{I}_1^{\,2} - 9\right) + \frac{11}{1050N^2}\left(\bar{I}_1^{\,3} - 27\right) + \frac{19}{7000N^3}\left(\bar{I}_1^{\,4} - 81\right) + \frac{519}{673750N^4}\left(\bar{I}_1^{\,5} - 243\right)\right] + \frac{K}{2}(J-1)^2 \quad (20)$$

where G is the shear modulus, N is the number of statistical links, J is relative volume and K is the bulk modulus.

This model also showed that the adopted model successfully reflects the behaviour of tire rubbers even at relatively high temperatures and under a moderate finite deformation.

The polynomial model was discussed in the study of Rivlin and Saunders [45] as the strain-energy function:

$$W = \sum_{p,q=0}^{N} C_{pq}(I_1 - 3)^p (I_2 - 3)^q \quad (21)$$

with $C_{00} = 0$, which is a generalisation of the Mooney–Rivlin and neo-Hookean strain-energy functions.

Note that the invariant based formulation is valid for isotropic materials. However, rubber-like materials are often isotropic, and thus this approach is valid.

4.2. Material model parameters identification

In the first stage of preparation of the numerical model of the studied phenomenon, it was necessary to properly determine the material constants of the constitutive model, which can correctly describe the behaviour of the hyperelastic material. After reviewing the available models, two models that are commonly used in various types of analyses involving the use of the finite element method were selected, namely the polynomial and Arruda–Boyce models. To determine the values of both constitutive models, the curve-fitting technique was used. The principle underlying this method is the determination of the function describing the series of data in relation to which analyses are required – in this case, the strain and stress values obtained during the experimental tests – in the best possible way, concomitant with taking into account any predefined constraints.

In the case of the model described by Eq. (27), the values of all material constants (C_{10}, C_{01}, C_{11}, C_{20}, C_{02} and C_{30}) were determined, with the proviso that all values must be greater than 0. Such a limitation was adopted because negative values of the constants, despite potentially very good curve fitting, may lead to instability during numerical analyses [46]. The determined constant values are presented in Tab. 4.

The Arruda–Boyce material model requires a much smaller number of constants. In practice only two, in addition to density and bulk modulus, are needed: the shear modulus (G) and the number of statistical links (N). The constraint was that both values should be greater than 0 and we assumed that the number of statistical links should be an integer. The values determined for this constitutive model are presented in Tab. 5.

After determining all the necessary constants, a finite element method numerical model was constructed, which allowed for the numerical validation of the material model constants' correctness and evaluation of the difference in the stress values between the experimental tests and numerical analyses. A geometrical model of the used tensile sample was created, which was then discretised using fully integrated solid elements. In order to replicate the real test, the application of the loading and boundary conditions is made as similar as possible to that relevant to the actual tensile experiment. Since the study is static, it was decided to use the implicit scheme of integrating the equations of motion implemented in the LS-Dyna solver.

Tab. 4. Polynomial model constants obtained through curve-fitting technique

	Temp. (°C)	C_{10} (MPa)	C_{01} (MPa)	C_{11} (MPa)	C_{20} (MPa)	C_{02} (MPa)	C_{30} (MPa)
CR/NBR	50	0.53698	0.01331	0.00007	0.07965	0.00058	0.00002
	25	0.66766	0.00002	0.06605	0.05914	0.00034	0.00001
	0	0.52132	0.00905	0.24118	0.00868	0.00006	0.00000
	−25	0.53088	0.00810	0.01617	0.04099	0.79866	0.00017
NR	50	0.70485	0.00042	0.00002	0.01733	0.00043	0.00070
	25	1.06824	0.00000	0.00088	0.01164	0.00003	0.00083
	0	1.16694	0.00046	0.00047	0.00803	0.01057	0.00231
	−25	0.92199	0.00995	0.00013	0.07905	0.00002	0.00244
SBR	50	0.50133	0.01044	0.02173	0.04461	0.00002	0.00020
	25	1.16859	0.01050	0.01124	0.00014	0.00000	0.00161
	0	0.25955	0.01184	0.17839	0.04629	0.00006	0.00088
	−25	1.12534	0.00126	0.03109	0.04438	0.00001	0.00200
NR/SBR	50	0.82210	0.00085	0.02343	0.04706	0.00391	0.00001
	25	1.08278	0.00058	0.00000	0.02202	0.00058	0.00000
	0	1.17437	0.00013	0.01408	0.00726	0.00055	0.00214
	−25	0.92199	0.00995	0.00013	0.07905	0.00002	0.00244

CR, chloroprene rubber; NBR, nitrile-butadiene rubber; NR, natural rubber; SBR, styrene-butadiene rubber.

Tab. 5. Arruda–Boyce constitutive material model constants obtained through curve-fitting technique

	Temp. (°C)	N (-)	G (MPa)
NR	50	7	1.33213
	25	12	1.92605
	0	6	1.66705
	-25	5	1.86775
CR/NBR	50	3	1.03194
	25	4	1.53908
	0	6	1.93717
	-25	9	2.90620
SBR	50	4	1.02686
	25	6	1.62532
	0	6	1.55613
	-25	6	2.18831
NR/SBR	50	5	1.58015
	25	5	1.61376
	0	7	1.99259
	-25	5	2.1981

CR, chloroprene rubber; NBR, nitrile-butadiene rubber; NR, natural rubber; SBR, styrene-butadiene rubber.

In total, a mesh of 6,080 elements is used for the analyses. The prepared numerical model is presented in Fig. 13. The constitutive model parameters are presented in Tabs. 4 and 5. The value of Poisson ratio was constant for every tested material and equal to 0.495.

The obtained results and comparison between the considered constitutive models are presented in Figs. 14a–d. To facilitate a comparison between the outcomes of the experimental tests and numerical analyses, the engineering values were transformed into true values by utilising the following set of formulae:

$$\varepsilon_{true} = \ln(1 + \varepsilon_{eng}) \tag{22}$$

$$\sigma_{true} = \sigma_{eng} * e^{\varepsilon_{true}} = \sigma_{eng} * (1 + \varepsilon_{eng}) \tag{23}$$

where ε_{true} represents true strain, ε_{eng} engineering strain, σ_{true} true stress, σ_{eng} engineering stress and e Euler's number.

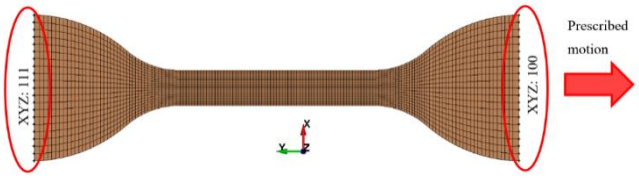

Fig. 13. Numerical model of the test sample with visible boundary conditions

When analysing the graphs in fig. 14, we can observe a high degree of agreement among the true-strain vs. true-stress curves representative of both constitutive models in the entire temperature range. Comparing them qualitatively, we can see that in most cases the curve representing the polynomial model coincides with the average curve obtained from the experimental test. The quantitative comparison of the obtained values of maximum true stress is presented in Tab. 6. Additionally, the difference between the experimental and numerical results is presented for both constitutive models. The average difference between the values obtained from the Arruda–Boyce model and experimental tests is about 16%, which is four times greater than from the polynomial model, where the difference is about 4%.

(a) CR/NBR

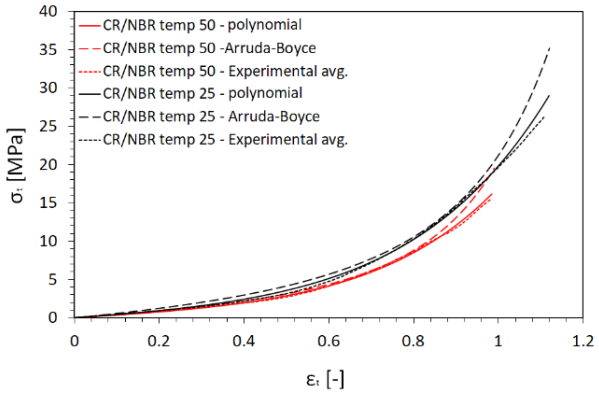

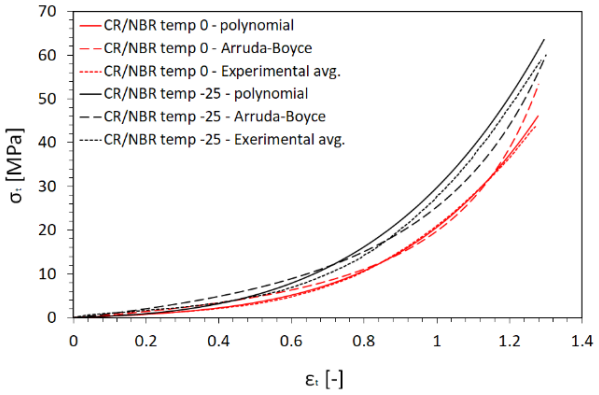

(b) NR

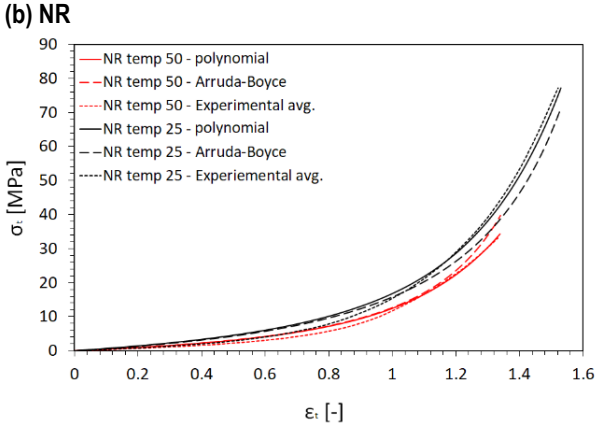

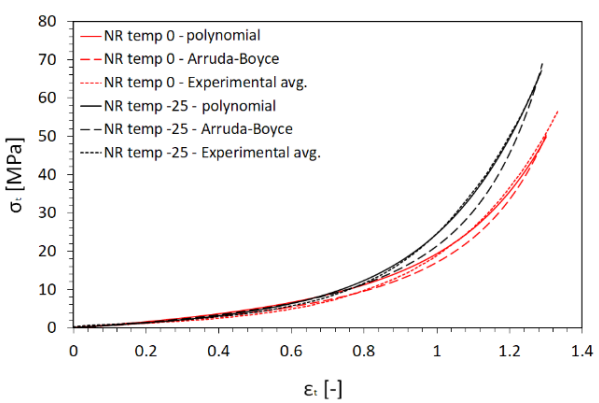

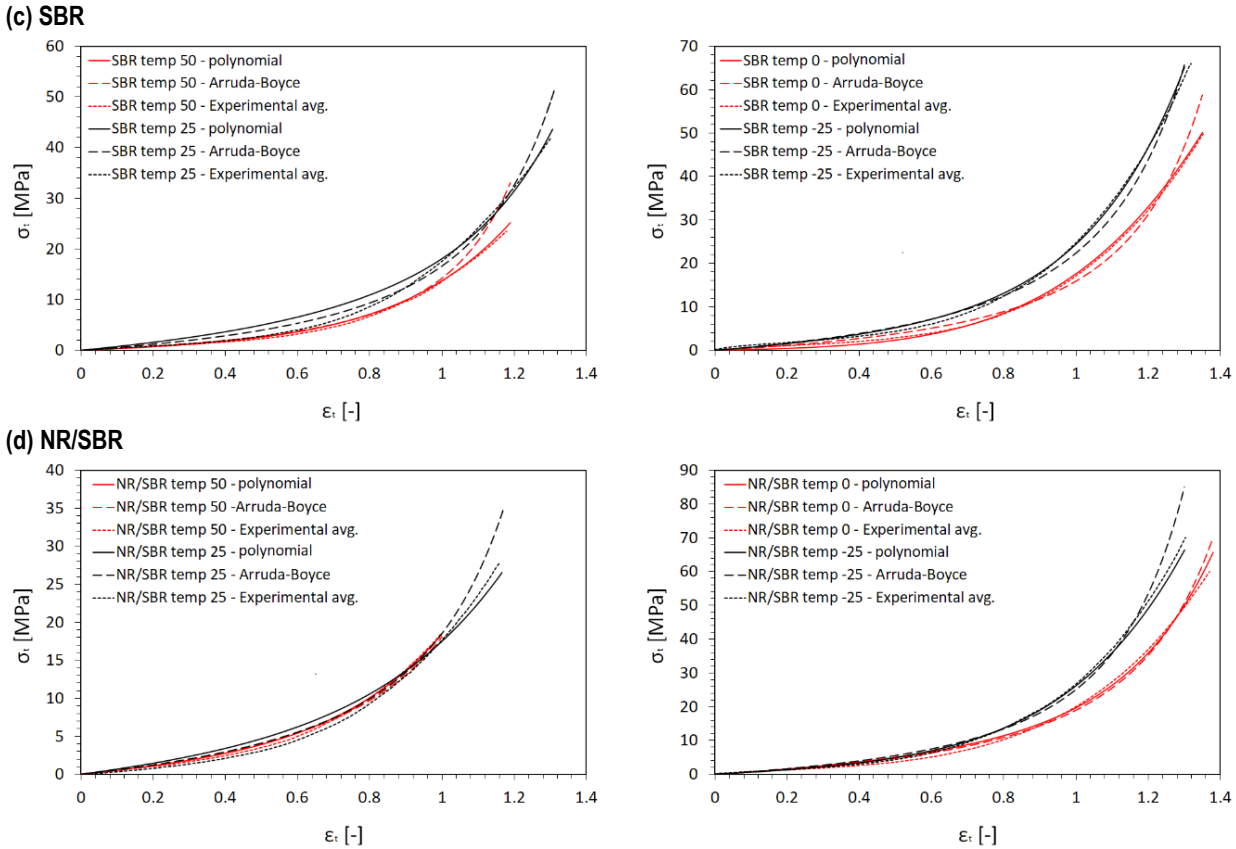

Fig. 14. True-strain vs. true-stress curves for polynomial and Arruda–Boyce material models in comparison with experimental results: a) CR/NBR, b) NR, c) SBR, d) NR/SBR. CR, chloroprene rubber; NBR, nitrile-butadiene rubber; NR, natural rubber; SBR, styrene-butadiene rubber.

Tab. 6. True stress obtained for constant true strain in every considered case

		True stress (MPa)				
		Exp. avg.	Polynomial	Arruda–Boyce	Polynomial diff. (%)	Arruda–Boyce diff. (%)
CR/NBR	50°C	15.42	16.15	19.55	4.73	26.78
	25°C	26.37	29.00	35.21	9.97	33.52
	0°C	43.69	46.08	53.40	5.47	22.22
	–25°C	58.85	63.57	60.06	8.02	2.06
NR	50°C	33.14	34.34	39.79	3.62	20.07
	25°C	77.08	77.18	71.06	0.13	7.81
	0°C	56.55	49.85	50.19	11.85	11.25
	–25°C	67.07	67.16	68.84	0.13	2.64
SBR	50°C	23.46	25.17	33.06	7.29	40.92
	25°C	41.77	43.97	51.16	5.27	22.48
	0°C	49.71	50.14	58.78	0.87	18.25
	–25°C	65.95	65.13	65.64	1.24	0.47
NR/SRB	50°C	18.56	18.33	18.05	1.24	2.75
	25°C	27.89	26.54	34.67	4.84	24.31
	0°C	59.96	65.66	69.93	9.51	16.63
	–25°C	70.08	66.39	85.04	5.27	21.35

4.3. Material model parameters calibration

The material model constants determined above served as a starting point for the optimisation process using the SRSM implemented in the LS-OPT software. SRSM is based on the response surface methodology (RSM), which is a statistical method for constructing approximations to the objective function in the multi-dimensional parameter space. In this approach, a design space is defined, and variable sets are selected within it:

$$G\ \overline{\overline{min}}\ \frac{1}{K}\sum_{i=1}^{K}\left[F_{exp}(\varepsilon_i) - F_{num}(\varepsilon_i)\right]^2 \tag{24}$$

where G is an objective function and K is the number of sampling points.

In the optimisation process, both variables and constraints were normalised, following the classical, commonly used approach:

– variable:

$$\gamma_i = \frac{x_i - x_{i\,min}}{x_{i\,max} - x_{i\,min}};\ \ i = 1,\ 2, \ldots \tag{25}$$

– constraints:

$$1 \geq \frac{g_j}{L_{max}};\ \ j = 1,\ 2, \ldots \tag{26}$$

$$0 \leq g_j;\ \ j = 1,\ 2, \ldots \tag{27}$$

The dynamic leapfrog method for constrained minimisation was used to solve the optimisation problem [47].

A series of finite element method analyses are performed for the variable combinations, the model response is calculated and polynomial functions are fitted to the previously selected variables [48]. In the SRSM, a sub-region is defined in the design space and the optimum is determined on the approximated response surface. In the subsequent step, a new region is defined in such a way that its centre is located on the previous successive optimum and its size is reduced [49].

The parameters obtained through optimisation process for both polynomial and Arruda–Boyce material models are presented in Tabs. 7 and 8.

The comparison between the true-strain and true-stress curves is depicted in Fig. 15. A significant degree of agreement is observed between the curves for the post-calibration models and the experimental curve. The polynomial model shows better agreement with the experimental data at higher true-strain values, particularly above the value of 1.2. However, despite the calibration process, the Arruda–Boyce model exhibits an overestimation of the true-stress values and an underestimation of the true-strain values for large strain values.

Tab. 7. Optimised material parameters for Arruda–Boyce constitutive model

	Temp.(°C)	N (-)	G (MPa)
NR	50	7	1.27683
	25	6	1.38102
	0	5	1.50824
	-25	4	1.50441
CR/NBR	50	4	1.23285
	25	5	1.51941
	0	5	1.68370
	-25	5	1.87934
SBR	50	6	1.18632
	25	6	1.56921
	0	6	1.44424
	-25	5	1.67927
NR/SBR	50	6	1.58506
	25	5	1.46674
	0	4	1.49668
	-25	4	1.46575

CR, chloroprene rubber; NBR, nitrile-butadiene rubber; NR, natural rubber; SBR, styrene-butadiene rubber.

Tab. 8. Optimised material parameters for polynomial constitutive material model

	Temp. (°C)	C_{10} (MPa)	C_{01} (MPa)	C_{11} (MPa)	C_{20} (MPa)	C_{02} (MPa)	C_{30} (MPa)
CR/NBR	50	0.11474	0.00001	0.37600	0.10684	0.04652	0.00024
	25	0.06402	0.31676	0.39453	0.10772	0.01939	0.00000
	0	0.00563	0.03458	0.36411	0.30683	0.00288	0.00000
	–25	0.04090	0.36302	0.62358	0.10171	0.04711	0.00000
NR	50	0.06811	0.04967	0.50681	0.00408	0.03136	0.00050
	25	0.18600	0.01373	0.42619	0.05592	0.03299	0.00055
	0	0.08466	0.02086	0.55986	0.09241	0.02707	0.00202
	–25	0.11986	0.04841	0.52687	0.02299	0.08504	0.00406
SBR	50	0.02147	0.00000	0.37557	0.05590	0.04300	0.00023
	25	0.02460	0.04584	0.43551	0.10649	0.04947	0.00000
	0	0.07404	0.01176	0.44553	0.04083	0.05496	0.00103
	–25	0.20000	0.00000	0.56579	0.09205	0.07829	0.00072
NR/SBR	50	0.04796	0.03702	0.60932	0.15244	0.00246	0.00000
	25	0.02381	0.05043	0.53841	0.18494	0.00000	0.00000
	0	0.11481	0.08666	0.56767	0.01504	0.06928	0.00000
	–25	0.19999	0.05387	0.52350	0.14427	0.07685	0.00051

(a) NR 50 °C

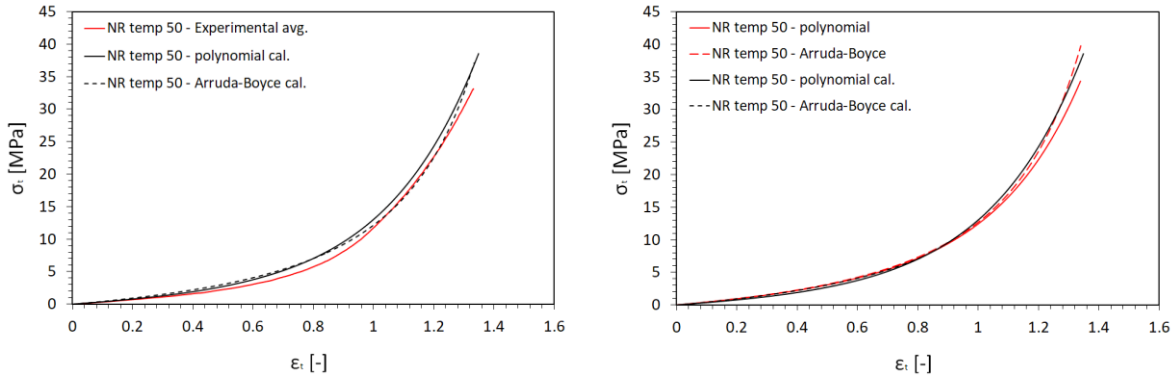

(b) NR 25 °C

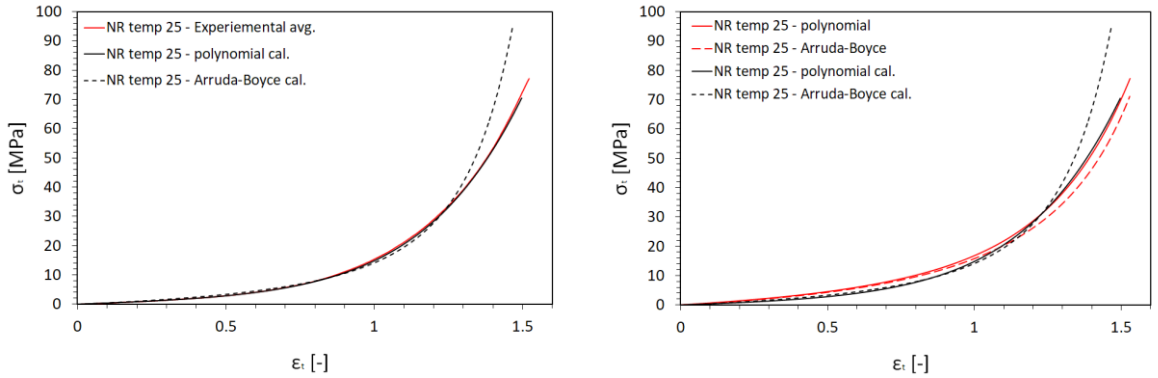

(c) NR 0 °C

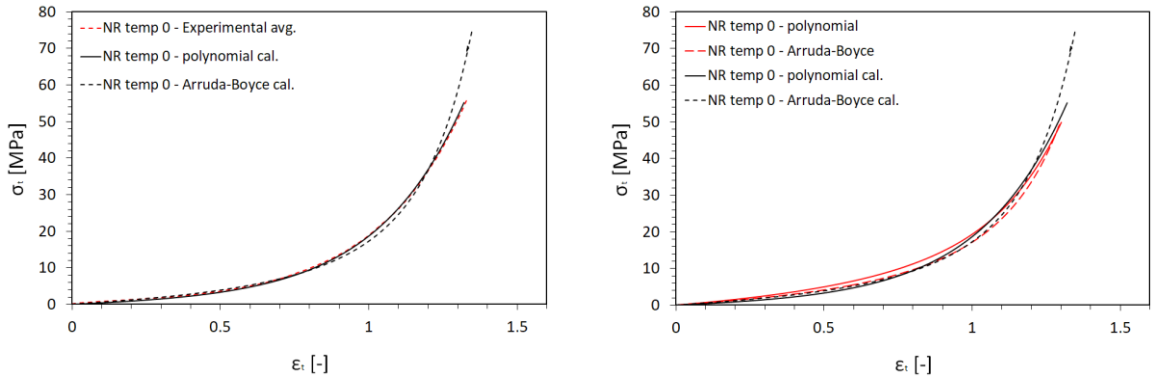

(d) NR –25 °C

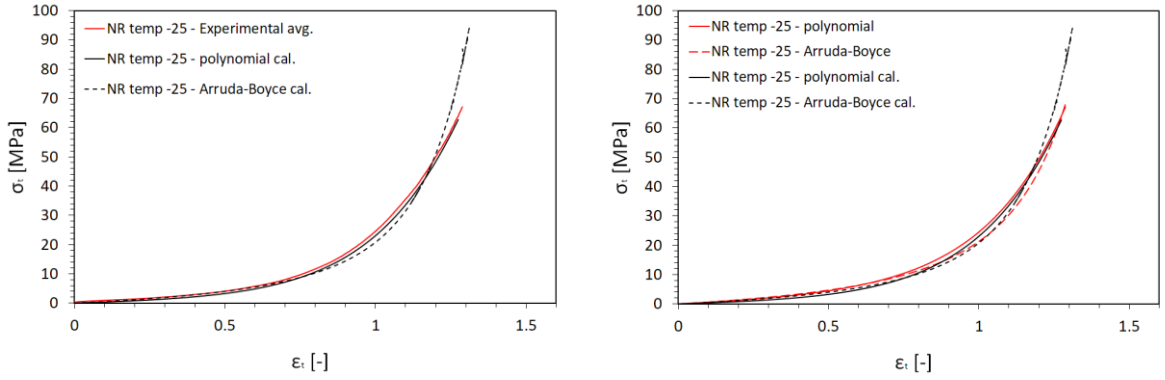

Fig. 15. Comparison of true-strain vs. true-stress curves for calibrated and non-calibrated polynomial and Arruda–Boyce models parameters for NR at temperatures: a) 50°C, b) 25°C, c) 0°C and d) -25°C. NR, natural rubber.

5. CONCLUSION

In conclusion, we report the change in the thermal and mechanical properties of several hyperelastic materials tested in the temperature ranging from −25°C up to 50°C. The results of the experimental tests show a significant change in the materials' behaviour, especially in the lowered temperatures.

Such changes in the properties of hyperelastic materials clearly shows that, in order to perform a correct numerical analysis of components prepared with the use of these materials, a wide range of the material parameters is necessary. There are a number of a constitutive material models that can be used to describe the behaviour of rubber-like materials; however, we have focused on the two most commonly used: the Arruda–Boyce and polynomial models. A combination of the experimental tests and the finite element method, along with the curve fitting, allowed for the determination of a set of material constants for both models for the whole considered temperature range. The performed analyses showed that for true-strain values above 1, the hyperelastic polynomial model provides a better representation of the material behaviour than the Arruda–Boyce model.

We believe that the determined parameters would be a great help for anybody interested in numerical simulations of the components made from rubber-like materials.

REFERENCES

1. Li X, Dong Y, Li Z, Xia Y. Experimental study on the temperature dependence of hyperelastic behavior of tire rubbers under moderate finite deformation. Rubber Chem Technol. 2011 Jun 1;84(2):215–28.
2. Gordon M. The Physics of Rubber Elasticity (Third Edition). L. R. G. Treloar, Clarendon Press, Oxford. 1975 pp. xii + 370. Br Polym J. 1976 Mar;8(1):39–39.
3. Bell CLM, Stinson D, Thomas AG. Measurement of Tensile Strength of Natural Rubber Vulcanizates at Elevated Temperature. Rubber Chem Technol. 1982 Mar 1;55(1):66–75.
4. Stevenson A. The influence of low-temperature crystallization on the tensile elastic modulus of natural rubber. J Polym Sci Polym Phys Ed. 1983 Apr;21(4):553–72.
5. D20 Committee. Test Method for Brittleness Temperature of Plastics and Elastomers by Impact [Internet]. ASTM International; [cited 2023 May 29]. http://www.astm.org/cgi-bin/resolver.cgi?D746-20
6. Hussein M. Effects of strain rate and temperature on the mechanical behavior of carbon black reinforced elastomers based on butyl rubber and high molecular weight polyethylene. Results Phys. 2018 Jun;9:511–7.
7. Barlow C, Jayasuriya S, Suan Tan C. The World Rubber Industry [Internet]. 0 ed. Routledge; 2014 [cited 2023 May 29]. https://www.taylorfrancis.com/books/9781317829133
8. McKeen LW. Elastomers and Rubbers. In: The Effect of UV Light and Weather on Plastics and Elastomers [Internet]. Elsevier; 2019 [cited 2023 May 29]. p. 279–359. https://linkinghub.elsevier.com/retrieve/pii/B9780128164570000101
9. Ramesan MT, Anil Kumar T. Preparation And Properties Of Different Functional Group Containing Styrene Butadiene Rubber. J Chil Chem Soc [Internet]. 2009 [cited 2023 May 29];54(1). http://www.scielo.cl/scielo.php?script=sci_arttext&pid=S0717-97072009000100006&lng=en&nrm=iso&tlng=en
10. Chandrasekaran VC. Rubbers, Chemicals and Compounding for 'O' Rings and Seals. In: Rubber Seals for Fluid and Hydraulic Systems [Internet]. Elsevier; 2010 [cited 2023 May 29]. p. 57–69. https://linkinghub.elsevier.com/retrieve/pii/B9780815520757100061
11. Guo L, Huang G, Zheng J, Li G. Thermal oxidative degradation of styrene-butadiene rubber (SBR) studied by 2D correlation analysis and kinetic analysis. J Therm Anal Calorim. 2014 Jan;115(1):647–57.
12. Kurian T, Mathew NM. Natural Rubber: Production, Properties and Applications. In: Kalia S, Avérous L, editors. Biopolymers [Internet]. Hoboken, NJ, USA: John Wiley & Sons, Inc.; 2011 [cited 2023 May 29]. p. 403–36. https://onlinelibrary.wiley.com/doi/10.1002/9781118164792.ch14
13. Kobayashi S, Müllen K, editors. Encyclopedia of Polymeric Nanomaterials [Internet]. Berlin, Heidelberg: Springer Berlin Heidelberg; 2015 [cited 2023 May 29]. http://link.springer.com/10.1007/978-3-642-29648-2
14. P M, Te M. Natural Rubber and Reclaimed Rubber Composites–A Systematic Review. Polym Sci [Internet]. 2016 [cited 2023 May 29];2(1). http://polymerscience.imedpub.com/natural-rubber-and-reclaimed-rubber-compositesa-systematic-review.php?aid=11066
15. Chandrasekaran C. Anticorrosive rubber lining: a practical guide for plastics engineers. Oxford: Elsevier; 2017. 266 p. (Plastics design library).
16. Thomas S, editor. Progress in rubber nanocomposites. Amsterdam: Elsevier; 2017. 574 p. (Woodhead Publishing series in composites science and engineering).
17. Huang Y, Li Y, Zhao H, Wen H. Research on constitutive models of hydrogenated nitrile butadiene rubber for packer at different temperatures. J Mech Sci Technol. 2020 Jan;34(1):155–64.
18. Bauccio M, American Society for Metals, editors. ASM metals reference book. 3rd ed. Materials Park, Ohio: ASM International; 1993.
19. Ismail MN, El-Sabbagh SH, Yehia AA. Fatigue and Mechanical Properties of NR/SBR and NR/NBR Blend Vulcanizates. J Elastomers Plast. 1999 Jul;31(3):255–70.
20. Ward IM, Sweeney J. Mechanical Properties of Solid Polymers: Third Edition [Internet]. 1st ed. Wiley; 2012 [cited 2023 May 29]. https://onlinelibrary.wiley.com/doi/book/10.1002/9781119967125
21. Copley BC. Tackification Studies of Natural Rubber/Styrene-Butadiene Rubber Blends. Rubber Chem Technol. 1982 May 1;55(2):416–27.
22. Zeng X, Li G, Zhu J, Sain M, Jian R. NBR/CR-Based High-Damping Rubber Composites Containing Multiscale Structures for Tailoring Sound Insulation. Macromol Mater Eng. 2023 Feb;308(2):2200464.
23. Tobajas R, Ibartz E, Gracia L. A comparative study of hyperelastic constitutive models to characterize the behavior of a polymer used in automotive engines. In: Proceedings of 2nd International Electronic Conference on Materials [Internet]. Sciforum.net: MDPI; 2016 [cited 2023 May 29]. p. A002. http://sciforum.net/conference/ecm-2/paper/3398
24. Saha S, Bal S. Detailed study of dynamic mechanical analysis for nanocomposites. Emerg Mater Res. 2019 Sep 1;8(3):408–17.
25. Jose Chirayil C, Abraham J, Kumar Mishra R, George SC, Thomas S. Instrumental Techniques for the Characterization of Nanoparticles. In: Thermal and Rheological Measurement Techniques for Nanomaterials Characterization [Internet]. Elsevier; 2017.. https://linkinghub.elsevier.com/retrieve/pii/B9780323461399000013
26. Gill P, Moghadam TT, Ranjbar B. Differential scanning calorimetry techniques: applications in biology and nanoscience. J Biomol Tech JBT. 2010 Dec;21(4):167–93.
27. Leyva-Porras C, Cruz-Alcantar P, Espinosa-Solís V, Martínez-Guerra E, Piñón-Balderrama CI, Compean Martínez I, et al. Application of Differential Scanning Calorimetry (DSC) and Modulated Differential Scanning Calorimetry (MDSC) in Food and Drug Industries. Polymers. 2019 Dec 18;12(1):5.
28. Gallagher P. K., Brown M. E., Kemp R. B. Handbook of Thermal Analysis and Calorimetry. Amsterdam [Netherlands] ; New York: Elsevier; 1998.
29. Loos K, Aydogdu AB, Lion A, Johlitz M, Calipel J. Strain-induced crystallisation in natural rubber: a thermodynamically consistent model of the material behaviour using a serial connection of phases. Contin Mech Thermodyn. 2021 Jul;33(4):1107–40.

30. Wood L. A.,, Bekkedahl N. Crystallization of Unvulcanized Rubber at Different Temperatures. Journal of Applied Physics 17. 1946;362–75.
31. Doherty WOS, Leè KL, Treloar LRG. Non-Gaussian effects in styrene-butadiene rubber: Non-Gaussian effects in styrene-butadiene rubber. Br Polym J. 1980 Mar;12(1):19–23.
32. Schieppati J, Schrittesser B, Wondracek A, Robin S, Holzner A, Pinter G. Temperature impact on the mechanical and fatigue behavior of a non-crystallizing rubber. Int J Fatigue. 2021 Mar;144:106050.
33. Mooney M. A Theory of Large Elastic Deformation. J Appl Phys. 1940 Sep;11(9):582–92.
34. Large elastic deformations of isotropic materials IV. further developments of the general theory. Philos Trans R Soc Lond Ser Math Phys Sci. 1948 Oct 5;241(835):379–97.
35. Peddini SK, Bosnyak CP, Henderson NM, Ellison CJ, Paul DR. Nanocomposites from styrene–butadiene rubber (SBR) and multiwall carbon nanotubes (MWCNT) part 2: Mechanical properties. Polymer. 2015 Jan;56:443–51.
36. Tzounis L, Debnath S, Rooj S, Fischer D, Mäder E, Das A, et al. High performance natural rubber composites with a hierarchical reinforcement structure of carbon nanotube modified natural fibers. Mater Des. 2014 Jun;58:1–11.
37. Kondyurin A, Eliseeva A, Svistkov A. Bound ("Glassy") Rubber as a Free Radical Cross-linked Rubber Layer on a Carbon Black. Materials. 2018 Oct 16;11(10):1992.
38. Fröhlich J, Niedermeier W, Luginsland HD. The effect of filler–filler and filler–elastomer interaction on rubber reinforcement. Compos Part Appl Sci Manuf. 2005 Apr;36(4):449–60.
39. Mechanics of Solid Polymers [Internet]. Elsevier; 2015. https://linkinghub.elsevier.com/retrieve/pii/C20130154931
40. Darijani H, Naghdabadi R, Kargarnovin MH. Hyperelastic materials modelling using a strain measure consistent with the strain energy postulates. Proc Inst Mech Eng Part C J Mech Eng Sci. 2010 Mar 1;224(3):591–602.
41. Yeoh OH. Characterization of Elastic Properties of Carbon-Black-Filled Rubber Vulcanizates. Rubber Chem Technol. 1990 Nov 1;63(5):792–805.
42. Arruda EM, Boyce MC. A three-dimensional constitutive model for the large stretch behavior of rubber elastic materials. J Mech Phys Solids. 1993 Feb;41(2):389–412.
43. Treloar LRG. The elasticity of a network of long-chain molecules—II. Trans Faraday Soc. 1943;39(0):241–6.
44. Zhang MG, Cao YP, Li GY, Feng XQ. Spherical indentation method for determining the constitutive parameters of hyperelastic soft materials. Biomech Model Mechanobiol. 2014 Jan;13(1):1–11.
45. Large elastic deformations of isotropic materials VII. Experiments on the deformation of rubber. Philos Trans R Soc Lond Ser Math Phys Sci. 1951 Apr 24;243(865):251–88.
46. Hallquist, J.O. Ls-Dyna. Material Manual. 2005;
47. Stander N, Craig K.J, Reichert R. Material identification in structural optimization using response surfaces. Struct Multidiscip Optim. 2005 Feb;29(2):93–102.
48. Snyman JA. The LFOPC leap-frog algorithm for constrained optimization. Comput Math Appl. 2000 Oct;40(8–9):1085–96.
49. Mullerschön H, Thiele M. Optimization of an Adaptive Restraint System Using LS-OPT and Visual Exploration of the Design Space Using D-SPEX. 2006;

This research was funded under the Project of the Ministry of National Defense of the Republic of Poland Program – Research Grant (GBMON/13-999/2018/WAT), and the article was written as part of the implementation of the university research grant No. 22-874 of Military University of Technology.

Marcin Konarzewski: https://orcid.org/0000-0003-3352-8621
Michał Stankiewicz: https://orcid.org/0000-0003-1925-5292
Marcin Sarzyński: https://orcid.org/0000-0003-3561-6123
Marcin Wieczorek: https://orcid.org/0000-0002-0297-535X
Magdalena Czerwińska: https://orcid.org/0000-0002-7968-5019
Piotr Prasuła: https://orcid.org/0000-0001-5053-2046
Robert Panowicz: https://orcid.org/0000-0002-0709-1369

This work is licensed under the Creative Commons BY-NC-ND 4.0 license.